Molecular Gelation-Induced Functional Phase Separation in Polymer Film for Energy Transfer Spectral Conversion

*Hirokuni Jintoku, Miho Yamaguchi, Makoto Takafuji, and Hirotaka Ihara**

A new strategy for creating the energy transfer spectral conversion thin film by using fluorophore-functionalized molecular gelation is proposed. This is based on the facts that nanofibrillar phase separation of the self-assembling pyrene derivative as a fluorophore is formed in a bulk polymer-containing organic gel, and consequently that the phase-separated nano domain in a polymer thin film is enough small to keep the transparency but also extremely high Storks shift is gained by efficient excimer formation through highly ordered stacking among the pyrene moieties. When the phase separation-mediated functional polymer is applied as spectral conversion films (SCFs) for copper–indium–gallium–selenide (CIGS) solar cell, the SCF-covered solar cell exhibits significant improvement of power conversion efficiency by increase of photocurrent. In this paper, the FRET efficiency and emission wavelength are also demonstrated to be thermotropically switchable since order-to-disordered transitions are essential characteristics of as non-covalent low molecular assembling.

1. Introduction

Solar energy conversion plays an important role in producing vital life energy, and is a potential replacement for fossil fuel as a major energy source responsible for sustaining life and meeting societal demands. Solar energy must be efficiently harvested before it can be converted to various types of energy such as light, electricity, heat, chemicals, and so forth. Toward this goal, many types of silicone-based solar cells have been developed, consisting of single-crystal, multi-crystal, and amorphous structures such as compound semiconductive materials (e.g., CIGS, GaAs, and CdTe) or organic thin-layer-based materials.[1] However, all of these solar cells have a disadvantage, in that the photoreceptors cannot absorb the entire wavelength range of sunlight, which leads to inefficient energy conversion.

Not only is light-conversion efficiency significantly lower in the UV and IR regions than it is in the visible region (e.g., even plants cannot use UV wavelengths for photosynthesis),[2] but also strong UV light causes the solar cell to gradually deteriorate; one reasonable solution in overcoming this challenge is to pursue spectral conversion from the visible bands rather than direct UV conversion. Spectral conversion technology is the best-known candidate for this task. Therefore, several types of spectral conversion materials have been developed, which contain various fluorescent materials, including monomeric and polymeric dyes,[3] organometallic complexes,[4] and quantum dots.[5] However, spectral conversion films (SCFs) still have several disadvantages, such as low conversion efficiency, high fabrication cost, and poor durability.

Herein, we propose a new strategy for spectral conversion through efficient energy transfer in a phase-separated nano-sized functional domain. Our approach can be defined as utilization of a highly oriented nano-sized phase separation in a polymer matrix using a low-molecular gelation technique.[6] The nano-sized domain is induced by using self-assembling of organogelators as monomer components that can form one-dimensional fiber-like aggregates through intermolecular hydrogen bonding in a polymer matrix (**Figure 1**).[7] This method has several advantages in the fabrication of SCF materials: 1) the produced polymer film is transparent because our method does not generate macro-scale domains in the film, which cause light scattering, but instead forms nanofibrillar aggregates; 2) self-assembling phase separation is accompanied by molecular concentration and fluorescent group orientation, which promotes excimer formation and fluorescence resonance energy transfer (FRET) processes; 3) tunability of the fluorescent spectral band can be accomplished by a sol-to-gel transition.

We chose the L-glutamide derivative[8] for the purposes of fabricating this system, as such species have good dispersity in a variety of solvents, sufficient miscibility with polymeric materials,[9] and considerably low critical aggregation concentrations. Furthermore, their gelation properties and fluorescence behaviors in organic media have been extensively investigated by doping L-glutamide derivatives with fluorescent groups such as pyrene,[10] thiophene,[11] and porphyrin.[12] In this study, we have prepared the L-glutamide-functionalized pyrene (***g*-Pyr**) for use as the low-molecular-weight organogelator and fluorescent dyes (Coumarin 6, Rubrene and Nile red) as the energy acceptor for FRET.

Dr. H. Jintoku, M. Yamaguchi,
Dr. M. Takafuji, Prof. H. Ihara
Department of Applied Chemistry & Biochemistry
Kumamoto University
Kumamoto 860–8555, Japan
E-mail: ihara@kumamoto-u.ac.jp
Dr. M. Takafuji, Prof. H. Ihara
Kumamoto Institute for
Photo-Electro Organics (PHOENICS)
Kumamoto 862–0901, Japan

DOI: 10.1002/adfm.201304081

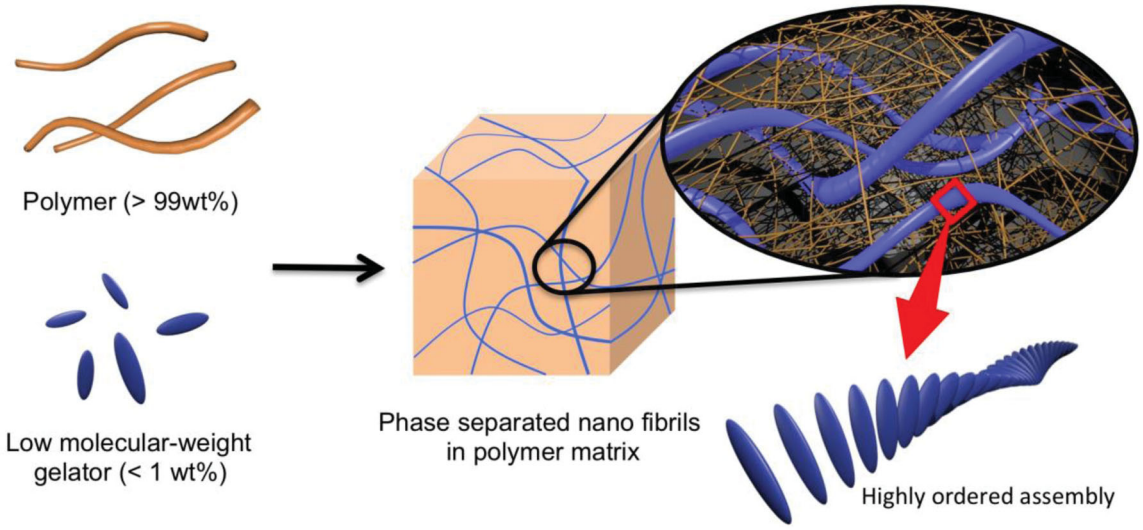

Figure 1. Schematic illustration of functional phase separated nano domain formation through highly ordered fibrous assembling.

2. Results and Discussion

2.1. Self-Assembly in Polymer Film

L-Glutamide-derived pyrene (***g*-Pyr**) was synthesized according to a reported procedure with slight modification.[10a] 1-Pyrenebutyric acid (**Pyr**) and poly(ethylene-*co*-vinyl acetate) (EVA) were selected as the non-assembling dye and polymer matrix, respectively. After preparing a mixed solution of toluene/ethyl acetate with ***g*-Pyr** and EVA, the solution was cast onto a glass plate to yield a pyrene-containing polymer film; its UV-vis, circular dichroism (CD) and fluorescence spectra were then measured (**Figure 2**). In the fluorescence spectrum, a maximum fluorescence wavelength was observed at 450 nm, which was attributable to excimer formation. The excimer formation rate I_{450}/I_{380} (fluorescent intensity of excimer at 450 nm vs that of monomer at 380 nm) was higher (I_{450}/I_{380} = 6.4) than that of the **Pyr**-incorporated EVA film (I_{450}/I_{380} = 0.23), indicating that most of the pyrene sites were aggregated in EVA via the L-glutamide unit. In the UV-vis and CD spectra, a red shift in the absorption band and positive Cotton effect were observed at 360 nm, indicating that the pyrene sites are slipped face-to-face (*J*-type) and chirally oriented (*R*-chiral). As a result, ***g*-Pyr** is considered to be in a highly oriented state that is induced through nano-sized phase separation within the EVA film.

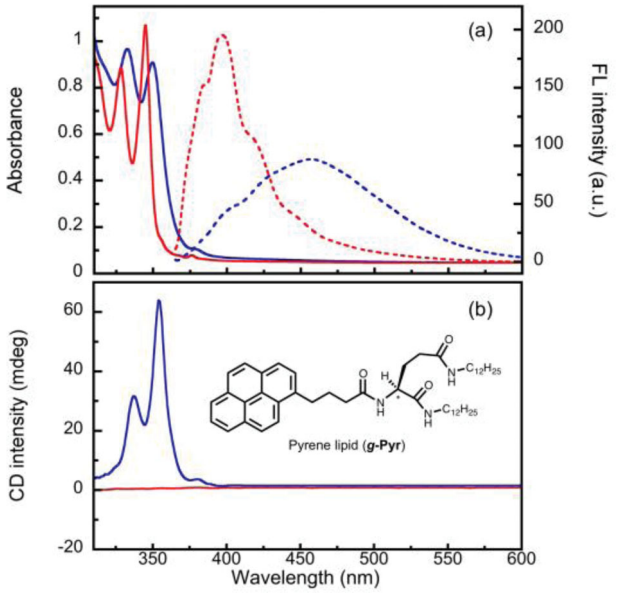

Figure 2. a) UV-vis (solid line) and fluorescence (dashed line) and b) CD spectra of ***g*-Pyr** (0.67 wt%) and **Pyr** (0.26 wt%) incorporated EVA film. The inset shows chemical structure of ***g*-Pyr**.

Transmission electron microscopy (TEM) was next used to observe the aggregation of ***g*-Pyr** for direct measurement of the phase-separated domain in the EVA film (**Figure 3**). Ruthenium(II) tetraacetate was used as the staining agent for TEM sample preparation to selectively stain the aromatic rings. The black regions observed in the TEM photographs were composed of ***g*-Pyr** aggregates consisting of nanofibers of 10 nm width and lengths ranging from several tens of nanometers to several micrometers. Additionally, some portions of the ***g*-Pyr** aggregates showed a right-handed helical structure. These images obviously indicate that ***g*-Pyr** forms a phase-separated nano-sized helical domain in the polymer matrix.

2.2. Self-Assembly in Organic Solution

A detailed investigation into the orientation of the ***g*-Pyr** assembly in the polymer matrix was next conducted (Figure S1, Supporting Information). To an EVA-containing toluene/ethyl acetate mixed solution was dissolved ***g*-Pyr** and **Pyr**; after dispersing by heating at 70 °C, the solution was quickly cooled to 10 °C to produce a gel. As shown in the UV-vis spectrum of ***g*-Pyr**/EVA gel, a 6 nm blue shift in the absorption band was observed, in contrast to that observed for the ***g*-Pyr**/EVA polymer film. The fluorescence spectrum exhibited an excimer emission; however, the excimer formation rate (I_{450}/I_{380}) was

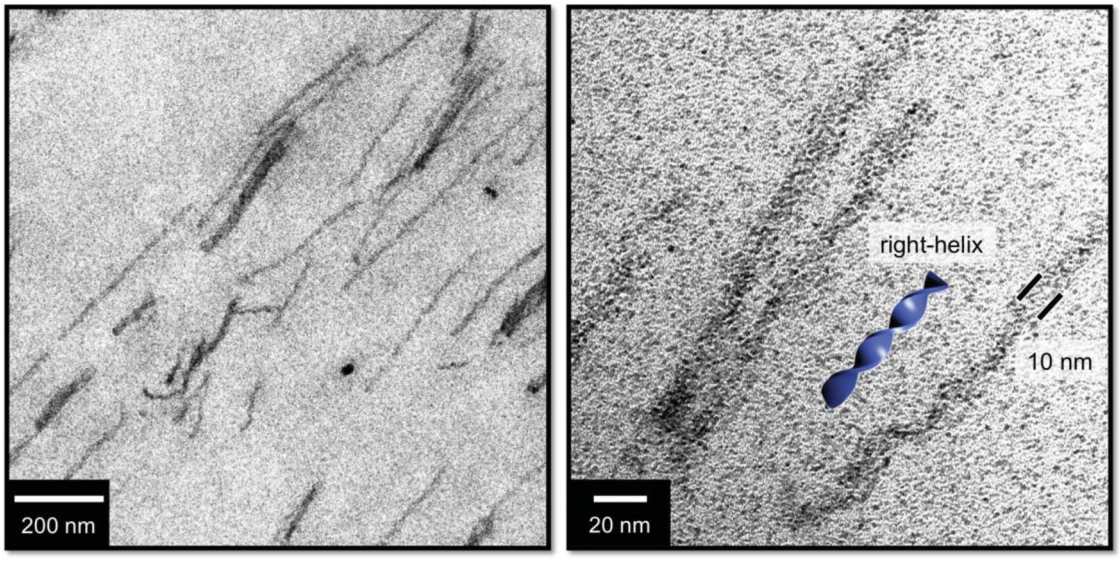

Figure 3. TEM images of ***g*-Pyr** (0.67 wt%) incorporated EVA film. Black parts: ***g*-Pyr**, white part: EVA.

lower than that of the ***g*-Pyr**/EVA film ($I_{450}/I_{380} = 3.3$), indicating that the molecular orientation of ***g*-Pyr** is promoted by phase-separation in the polymer matrix. In contrast, **Pyr** did not show such phenomena. Both states exhibited almost no absorption change and similar I_{450}/I_{380} values ($I_{450}/I_{380} = 0.29$ and 0.23 in solution and film, respectively), indicating molecular dispersion of the pyrene moiety. The ***g*-Pyr** materials also exhibited similar spectra at high temperature and in suitable solvents (e.g., chloroform and tetrahydrofuran).[10a] These results indicate that the nano-sized phase separation, which promotes molecular orientation, is produced by the self-assembling of L-glutamide units.

2.3. Energy Transfer System

The energy transfer properties were first evaluated in solution states to examine FRET-mediated spectral conversion processes. FRET, a highly important technology for fluorescent probe, sensor, and spectral conversion applications, occurs by a through-space (Förster) mechanism from donor molecules to an acceptor, with the following requirements: 1) the donor (or acceptor) molecules must be in close proximity to one other (generally 20–60 Å, as long as 100 Å for efficient acceptors); 2) the acceptor absorption must overlap the fluorescence spectrum of the donor.[13] Many reports exist describing efficient FRET by using aggregated scaffolds such as organogel,[14] hydrogel,[15] DNA,[16] polymer,[17] low molecular,[18] and inorganic[19] materials.

Coumarin 6 (C6), Rubrene (Rub) and Nile red (NR) were selected as energy-acceptor molecules. At 10 °C, when the mixture of ***g*-Pyr** (0.5 mM) with C6 (0–20 mol%) was excited at 350 nm, a gradual decrease in excimeric emission (λ_{max} = 450 nm) was observed with an increase in a new emission band (λ_{max} = 492 nm) (**Figure 4**a), indicating energy transfer from the pyrene excimer to C6. A similar energy transfer phenomenon was not observed at 60 °C. When increasing the C6 concentration, a slight increase was observed in the new emission band (Figure 4b). These results are attributed to the excimeric emission of ***g*-Pyr**, which produces not only good overlap with the absorption bands of C6 and the pyrene moiety, but is also in close proximity with C6 in the phase-separated nano-domain. FRET efficiency (φ_T) at 10 °C (calculated according to the method described in the Experimental Section) was significantly higher than that at 60 °C (Figure 4b inset); at a 4 mol% C6 loading, the φ_T values were 0.61 and 0.05 at 10 °C and 60 °C, respectively. In contrast, an efficient φ_T value was not obtained in the case of **Pyr** with a 4 mol% C6 loading (φ_T = 0.12). These results indicate that the phase-separated ***g*-Pyr** assembly promotes efficient FRET. **Table 1** summarizes the φ_T values under several conditions. Highly oriented ***g*-Pyr**-mixed systems exhibited efficient FRET using Rub and NR instead of C6 (Figure S2, Supporting Information).

We also demonstrated that fluorescence spectra could be thermoreversibly controlled based on the fact that the L-glutamide moiety[12a] exhibits properties and behaviors similar to those of lipid bilayer membranes.[6a,20] A typical example is the thermotropic phase transition between ordered and disordered states of ***g*-Pyr**. Figure S3 (Supporting Information) shows the change in fluorescence of a ***g*-Pyr** (0.5 mM) and C6 (4 mol%) mixture as the temperature increases from 10 to 60 °C. A drastic decrease in the C6 fluorescence emission was observed with increasing temperatures compared to the ***g*-free Pyr** system. As shown in the fluorescence intensity plot at 485 nm (Supporting Information Figure S3b, inset), a remarkable folding point was observed at 45 °C. A temperature-dependent UV-vis and CD spectral change was also observed for the ***g*-Pyr**/C6 mixture at the 45 °C folding point, indicative of the sol-to-gel transition temperature of ***g*-Pyr** (Figure S4, Supporting Information). Fluorescence emission of C6 could be observed once again by decreasing the temperature.

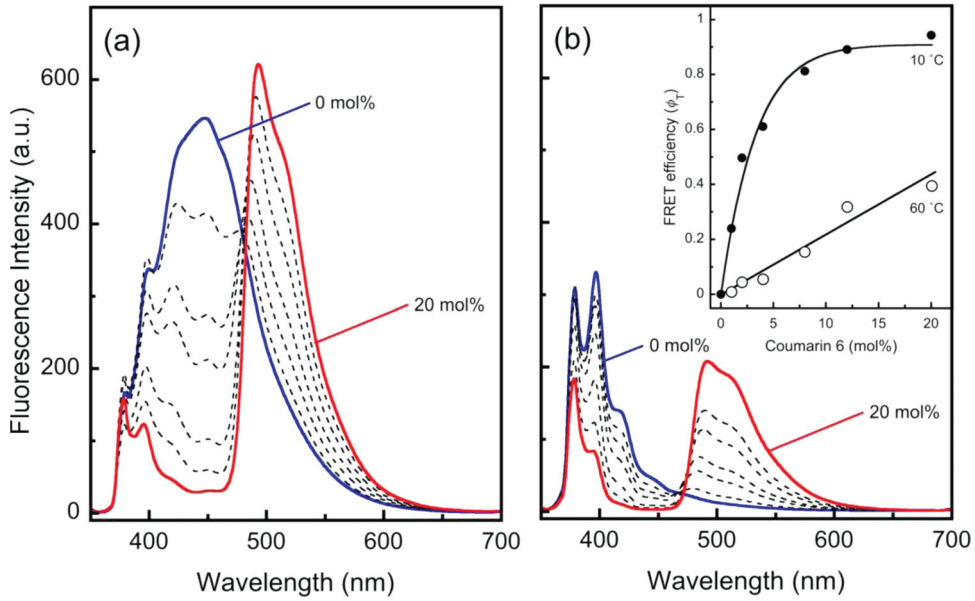

Figure 4. Fluorescence spectra of ***g*-Pyr** (0.5 mM) with C6 (0–20 mol%) and EVA_{40} (5 wt%) in a toluene/ethyl acetate (1 : 1) mixture at a) 10 °C and b) 60 °C. The inset shows concentration dependence of FRET efficiency (φ_T).

Figure 5 shows the corresponding temperature-dependent CIE 1931 chromaticity coordinates. Remarkably, emission color changes were observed for the ***g*-Pyr** self-assembled system with temperature change. In contrast, only a slight fluorescence color change was observed for **Pyr** in the dispersion states (Figure 5b). This result indicates that FRET in the self-assembling system has fluorescence color controllability due to not only energy transfer processes but also sol–gel transmission.

Energy-transfer SCF materials incorporating C6 and NR-doped ***g*-Pyr**/EVA films were fabricated by the same procedure as described above. Fluorescence spectral changes of C6 and the NR-doped ***g*-Pyr**/EVA film were observed as with the assembling state in solution (**Figure 6**). Moreover, the φ_T value was higher than that of the assembling state. This result suggests that the molecular distance between ***g*-Pyr** and C6 (or NR) is closer than that of the assembling state in solution due to phase-separated ***g*-Pyr** nano-domains in the polymer film. A lower FRET efficiency was observed using **Pyr** instead of ***g*-Pyr** as the non-assembling system (Figure 6b,d). **Table 2** summarizes φ_T values of films prepared under various conditions. In the film state, relatively high φ_T values were obtained compared with the assembling state in solution.

Table 1. FRET efficiency (φ_T) of various mixtures in solution.

Donor	Acceptor	Conc. [mol%]	Temp. [°C]	φ_T
Pyr	C6	4	10	0.12
			60	0.18
	Rub	20	10	0.05
			60	0.07
	NR	4	10	0.15
			60	0.15
***g*-Pyr**	C6	4	10	0.61
			60	0.06
		20	10	0.94
			60	0.40
	Rub	20	10	0.57
			60	0.15
	NR	4	10	0.30
			60	0.08

2.4. Application as Spectral Conversion Film

Spectral conversion properties were investigated by preparing SCFs under various conditions by the casting method onto glass (25 mm × 25 mm) and a copper–indium–gallium–selenide solar cell (CIGS, 25 mm × 25 mm) (Figure S5, Supporting

Table 2. FRET efficiency (φ_T) of various mixtures in polymer film.

Donor	Acceptor	Conc. [mol%]	φ_T
Pyr	C6	1	0.17
		4	0.44
		10	0.64
	NR	1	0.07
		4	0.18
***g*-Pyr**	C6	1	0.74
		4	0.74
		10	0.83
	NR	1	0.42
		4	0.63

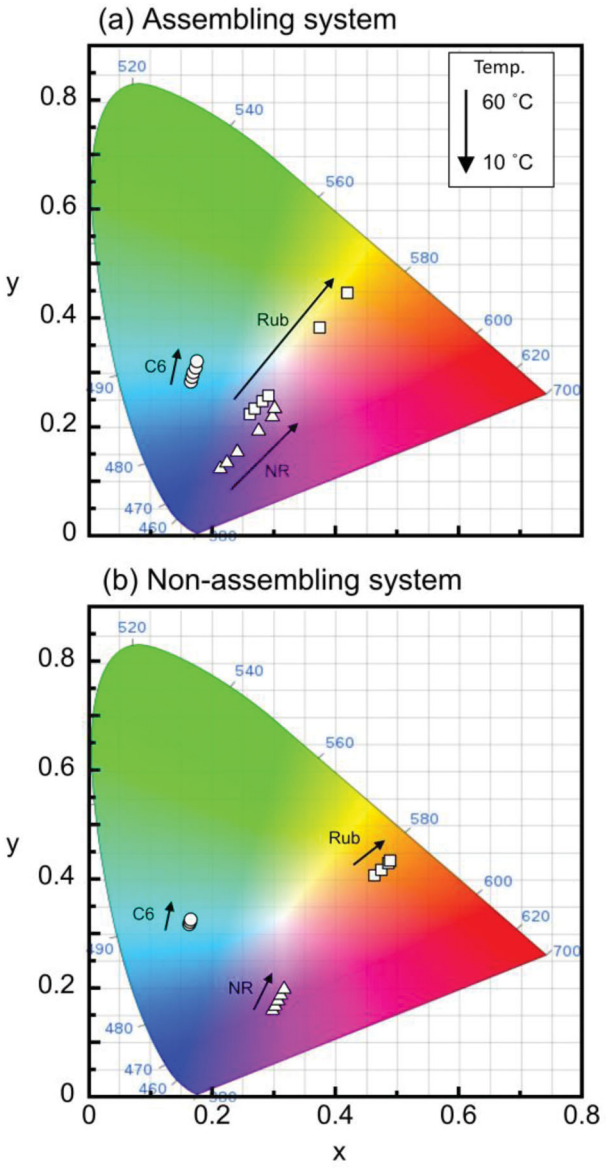

Figure 5. Temperature dependent corresponding CIE 1931 chromaticity coordinates of a) ***g*-Pyr** (0.5 mM) with acceptor dyes and EVA_{40} (5 wt%), and b) **Pyr** (0.5 mM) with acceptor dyes and EVA_{40} (5 wt%) in a toluene/ethyl acetate (1 : 1) mixture. Acceptor concentrations: C6 (4 mol%), NR (10 mol%), and Rub (200 mol%). The arrows indicate temperature change from 10 to 60 °C.

Information). Power-conversion efficiency was then calculated from current–voltage curves (**Figure 7**). **Table 3** summarizes the increase in rate of conversion efficiency ($\Delta\eta$) and the short-circuit current (ΔJ_{SC}) for the SCF-covered cell, as well as for the bare cell.

In our previous work, we reported the increase in power conversion efficiency of an amorphous silicone solar cell using a ***g*-Pyr**/polystyrene film.[9b] In the case of the as-prepared CIGS solar cell, we also observed an increase in power-conversion efficiency using the ***g*-Pyr**/EVA film (ΔJ_{SC} = 2.68%, $\Delta\eta$ = 3.57%). The highest power-conversion efficiency was observed for the 1 mol% C6-doped ***g*-Pyr**/EVA film-covered cell (η = 15.77%). This film exhibited an improvement in power-conversion efficiency of 4.85% compared to the bare cell (η = 15.04%). It was found that only J_{SC}, a property essential to power-conversion efficiency, showed a significant increase (ΔJ_{SC} = 4.57%), while all other factors (open voltage (V_{OC}), and fill factor (FF)) remained relatively unchanged. This finding strongly supports the presumption that the increase in power-conversion efficiency was due to the spectral conversion effect of SCF from UV to visible light.[21] Figure 7b exhibits a C6 concentration-dependent $\Delta\eta$ change. A decrease in the $\Delta\eta$ value was observed when increasing the concentration of C6 (0–10 mol%); this might be caused by the strong C6 absorption band in the visible region (400–500 nm). Incident photon-to-current conversion (IPCE) value of the CIGS solar cell, an indicator of spectral sensitivity character, was quite low in the pyrene absorption region (300–350 nm, average IPCE <10%). However, in the C6 absorption region (400–500 nm), the average IPCE value was found to be more than 80%, a likely reason why the strong absorption band in the visible region decreases the power-conversion efficiency. Transmission and fluorescence spectra of the C6-doped ***g*-Pyr**/EVA film support this assumption. For example, 1 mol% C6-doped film showed high transparency in the visible region (T% = 80%). In contrast, 10 mol% C6-doped film showed low transparency (T% = 50%) in the visible region due to the strong absorption of C6 (Figure S6a,b, Supporting Information). For the same reason, NR-doped ***g*-Pyr**/EVA film did not exhibit an effective increase in power-conversion efficiency. In the absence of ***g*-Pyr**, no enhancement in the power-conversion efficiency was observed by addition of each dye (C6, NR and Rub) as an additive into an EVA film because of the extremely low concentration. Therefore, the significant increase of the power-conversion efficiency is not delivered by these additives but realized by cooperation of ***g*-Pyr** with the additives. On the other hand, the modified cells with **Pyr**/EVA, C6-doped **Pyr**/EVA, and NR-doped **Pyr**/EVA films showed slight increases in power-conversion efficiencies ($\Delta\eta$ = 1.24%, 0.49% and 0.29%, respectively), while the cell coated with only EVA showed no change.

Table 3. Comparison of the short circuit current density (J_{SC}) and power-conversion efficiency (η) of modified CIGS cells based on the bare cell.

	Acceptor [mol%]	J_{SC} [mA cm^{-2}]	ΔJ_{SC} (%)	η (%)	$\Delta\eta$ (%)
Bare cell[a)]	–	7.51	–	15.0	–
EVA	–	7.54	0.36	15.1	0.07
Pyr/EVA	–	7.57	0.76	15.2	1.24
	C6 (1)	7.57	0.78	15.1	0.49
	NR (1)	7.55	0.56	15.1	0.29
***g*-Pyr**/EVA	–	7.71	2.68	15.6	3.57
	C6 (1)	**7.86**	**4.57**	**15.8**	**4.85**
	C6 (2)	7.10	1.94	15.3	2.03
	C6 (10)	7.58	0.88	15.1	0.49
	NR (1)	7.66	1.99	15.3	1.60
	NR (10)	7.40	–1.42	14.8	–1.63

[a)]Standard.

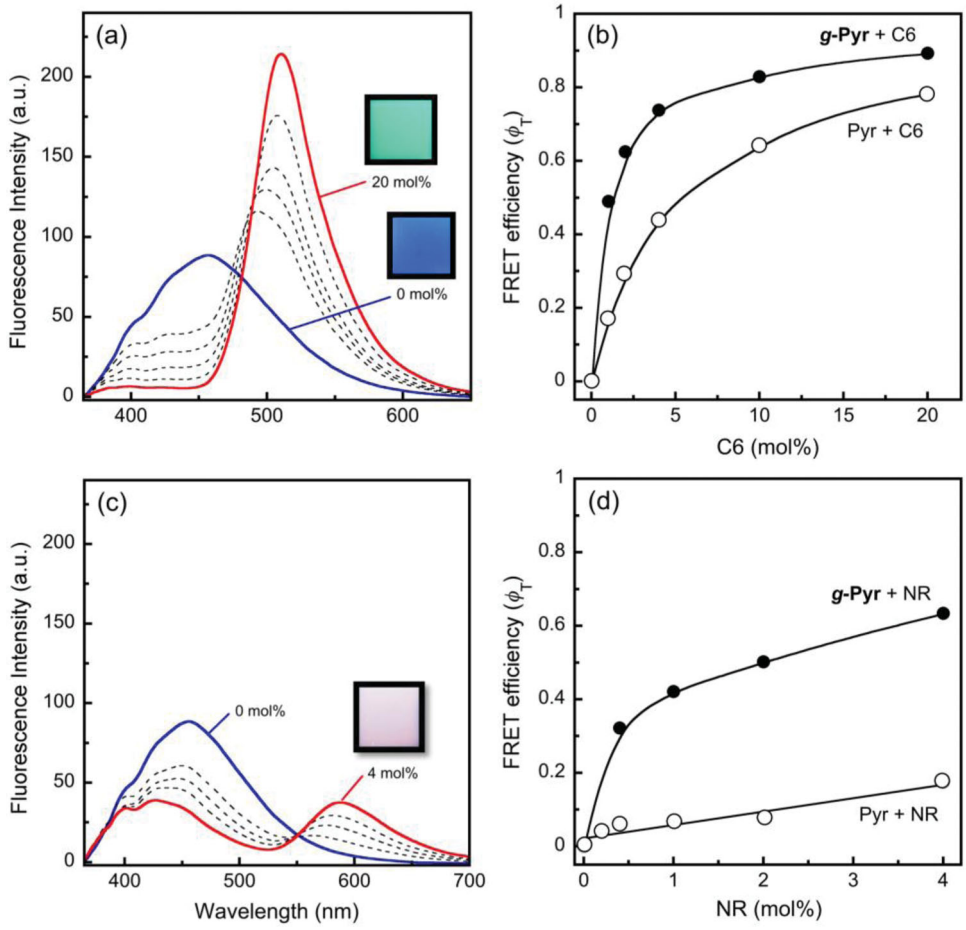

Figure 6. Concentration dependent fluorescence spectra of a) ***g*-Pyr**/C6 film and c) ***g*-Pyr**/NR film. Concentration dependent FRET efficiency change of b) ***g*-Pyr**/C6 and **Pyr**/C6, and (d) ***g*-Pyr**/NR and **Pyr**/NR. Dye concentrations: ***g*-Pyr** (0.67 wt%), **Pyr** (0.26 wt%), C6 (0–20 mol%), and NR (0–4 mol%).

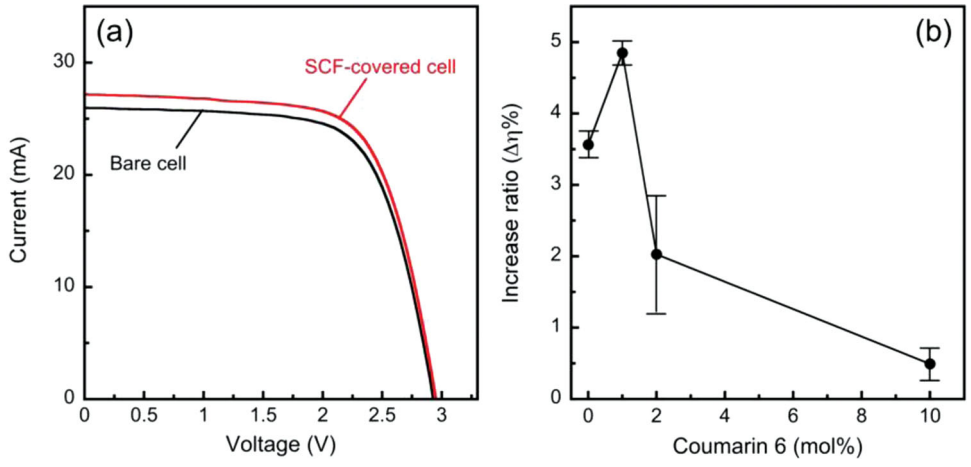

Figure 7. a) *I–V* curves of ***g*-Pyr**/C6 film-covered (red line) and non-covered (black line) CIGS solar cell. b) Increase ratio of power-conversion efficiency ($\Delta\eta$%) of ***g*-Pyr**/C6 film-covered CIGS solar cell versus C6 concentration.

The advantages of the phase-separated system were explained based on comparison of transmission and fluorescence spectra between C6-doped ***g*-Pyr**/EVA and **Pyr**/EVA films (Figure S6c, Supporting Information). A small amount (1 mol%) of C6-doped ***g*-Pyr**/EVA film showed strong fluorescence at 492 nm as C6 emission, due to efficient FRET in the phase-separated nano-domain. In contrast, in the case of **Pyr**/EVA film as non-assembling system, 4-fold C6 (4 mol%)

dopant loadings were required to obtain a similar fluorescence emission. However, as indicated in the above discussion it is expected that a large amount of C6 act as visible-light absorbents in decreasing the power-conversion efficiency. From these results, we may state that our phase-separated system, which provides control over emission wavelength by efficient FRET with addition of small amounts of acceptor molecules, is suitable for SCF.

3. Conclusion

In conclusion, we have established an energy-transfer spectral conversion process in a phase-separated nano-domain. The power-conversion efficiency of a CIGS solar cell was improved by addition of an SCF coating. A nano-sized phase-separation was accomplished by the self-assembling of an L-glutamide-derived lipid; furthermore, control of fluorescence emission was demonstrated by the addition of small amounts of acceptor dyes. This study demonstrates that the precisely designed SCFs, having suitable absorption and emission bands, can improve the power-conversion efficiencies of solar cells. Therefore, our method employing phase-separated nano-domains holds an advantage from the viewpoint of precise control of emission bands by excimer formation and efficient FRET. Further enhancement in the power-conversion efficiencies of various types of solar cells would be made possible by careful optimization of the absorption and emission wavelengths, especially in regards to dye concentration and variation. Such results could yield very promising and exciting advancements in the pursuit of alternative sources of energy.

4. Experimental Section

Materials: 25 mm × 25 mm CIGS solar cell (HEM135PCB) was supplied from Honda Soltec Co., Ltd. poly(ethylene-*co*-vinylacetate) (vinyl acetate: 40 wt%) and pyrene butyilic acid were purchased from Aldrich. Coumarin 6, Rublene, and Nile red were purchased from TCI. N^1,N^5-didodecyl-L-glutamide[10] and pyrene lipid (***g*-Pyr**) were synthesized by the previously reported procedure.

Instrumentation: UV-visible, CD and fluorescence spectra were measured with V-560 (JASCO), J725 (JASCO) and FP-6500 (JASCO), FP-8600 (JASCO), respectively. The photocurrent was measured under AM 1.5G illumination at 100 mW cm^{-2} under a XES–70S1 (SAN-EI ELECTRIC) solar simulator (7 cm × 7 cm photo-beam size). TEM images were observed with JEM-2100 (JEOL).

Calculation of FRET Efficiencies: FRET efficiencies (φ_T) were calculated according to[13]

$$\phi_T = 1 - \frac{I_{(D+A)}}{I_D}$$

in which $I_{(D+A)}$ is the fluorescence intensity of acceptor with ***g*-Pyr** (or **Pyr**) at 450 nm (or 380 nm). I_D is the fluorescence intensity of ***g*-Pyr** (or **Pyr**) at 450 nm (or 380 nm).

Supporting Information

Supporting Information is available from the Wiley Online Library or from the author.

Acknowledgements

This work was supported by an A-STEP; Adaptable and Seam-less Technology Transfer Program through Target-driven R&D (Exploratory Research), JST and a Grant-in-Aid for Program for Fostering Regional Innovation. The authors thank Satomi Nakagawa of Sekisui Chemical Co., Ltd. for TEM measurements. The authors also thank Keiko Kinoshita of Honda Soltec Co., Ltd. for provision of CIGS solar cells.

Received: December 5, 2013
Revised: January 16, 2014
Published online: April 1, 2014

[1] a) J. Zhao, A. Wang, M. A. Green, F. Ferrazza, *Appl. Phy. Lett.* **1998**, *73*, 1991–1993; b) G. A. Medvedkin, E. I. Terukov, Y. Hasegawa, K. Hirose, K. Sato, *Sol. Energy Mater. Sol. Cells* **2003**, *75*, 127–133; c) N. K. Subbaiyan, C. A. Wijesinghe, F. D'Souza, *J. Am. Chem. Soc.* **2009**, *131*, 14646–14647; d) J. L. Delgado, P-A. Bouit, S. Filippone, M. Herranza, N. Martin, *Chem. Commun.* **2010**, *46*, 4853–4865; e) Y. Liang, Z. Xu, J. Xia, S-T. Tsai, Y. Wu, G. Li, C. Ray, L. Yu, *Adv. Mater.* **2010**, *22*, 135–138; f) Y. Matsuo, Y. Sato, T. Niinomi, I. Soga, H. Tanaka, E. Nakamura, *J. Am. Chem. Soc.* **2009**, *131*, 16048–16050.

[2] a) G. McDermott, S. M. Prince, A. A. Freer, A. M. Hawthornthwaite-Lawless, M. Z. Papiz, R. J. Cogdell, N. W. Isaaca, *Nature* **1995**, *374*, 517–521; b) A. Egawa, T. Fujiwara, T. Mizoguchi, Y. Kakitani, Y. Koyama, H. Akutsu, *Proc. Natl. Acad. Sci. U.S.A.* **2007**, *104*, 790–795.

[3] a) H. J. Hovel, R. T. Hodgson, J. M. Woodall, *Sol. Energy Mater. Sol. Cells* **1979**, *2*, 19–29; b) W. G. J. H. M. van Sark, A. Meijerink, R. E. I. Schropp, J. A. M. van Roosmalen, E. H. Lysen, *Prog. Photovoltaics: Res. Appl.* **2011**, *19*, 345–351; c) G. C. Glaeser, U. Rau, *Thin Solid Films* **2007**, *515*, 5964–5967.

[4] a) O. Moudam, B. C. Rowan, M. Alamiry, P. Richardson, B. S. Richards, A. C. Jones, N. Robertson, *Chem. Commun.* **2009**, *43*, 6649–6651; b) T. Jin, S. Inoue, S. Tsutsumi, K. Machida, G. Adachi, *Chem. Lett.* **1997**, 171–172.

[5] W. G. J. H. M. van Sark, A. Meijerink, R. E. I. Schropp, J. A. M. van Roosmalen, E. H. Lysen, *Sol. Energy Mater. Sol. Cells* **2005**, *87*, 395–409.

[6] a) T. Kunitake, H. Ihara, Y. Okahata, *J. Am. Chem. Soc.* **1983**, *105*, 6070–6078; b) T. Kunitake, H. Ihara, Y. Okahata, *J. Am. Chem. Soc.* **1984**, *106*, 1156–1157.

[7] a) Y. Lin, R. G. Weiss, *Macromolecules* **1987**, *20*, 414–417; b) R. Oda, I. Huc, S. J. Cau, *Angew. Chem. Int. Ed.* **1998**, *37*, 2689–2691; c) M. Shirakawa, S. Kawano, N. Fujita, K. Sada, S. Shinkai, *J. Org. Chem.* **2003**, *68*, 5037–5044; d) M. Suzuki, T. Sato, A. Kurose, H. Shirai, K. Hanabusa, *Tetrahedron Lett.* **2005**, *46*, 2741–2745.

[8] a) H. Ihara, H. Hachisako, C. Hirayama, K. Yamada, *Chem. Commun.* **1992**, 1244–1245; b) H. Ihara, M. Takafuji, C. Hirayama, D. F. O'Brien, *Langmuir* **1992**, *8*, 1548–1553; d) X. Yang, G. Zhang, D. Zhang, D. Zhu, *Langmuir* **2010**, *26*, 11720–11725; e) Y. Li, M. Liu, *Chem. Commun.* **2008**, 5571–5573; f) X. Yang, G. Zhang, D. Zhang, J. Xiang, G. Yang, D. Zhu, *Soft Matt* **2011**, *7*, 3592–3598.

[9] a) M. Takafuji, Y. Kira, H. Tsuji, S. Sawada, H. Hachisako, H. Ihara, *Tetrahedron* **2007**, *63*, 7489–7494; b) H. Jintoku, H. Ihara, *Chem. Commun.* **2012**, *48*, 1297–1299; c) H. Jintoku, Y. Okazaki, M. Takafuji, H. Ihara, *Chem. Lett.* **2013**, *42*, 1297–1299.

[10] a) T. Sagawa, S. Fukugawa, T. Yamada, H. Ihara, *Langmuir* **2002**, *18*, 7223–7228; b) H. Ihara, T. Yamada, M. Nishihara, T. Sakurai, M. Takafuji, H. Hachisako, T. Sagawa, *J. Mol. Liq.* **2004**, *111*, 73–76.

[11] K. Miyamoto, T. Sawada, H. Jintoku, M. Takafuji, T. Sagawa, H. Ihara, *Tetrahedron Lett.* **2010**, *51*, 4666–4669.

[12] a) H. Jintoku, T. Sagawa, M. Takafuji, H. Ihara, *Org. Biomol. Chem.* **2009**, *7*, 2430–2434; b) H. Jintoku, T. Sagawa, T. Sawada, M. Takafuji, H. Ihara, *Org. Biomol. Chem.* **2010**, *8*, 1344–1350.
[13] a) G. Zaragoza-Galán, M. A. Fowler, J. Duhamel, R. Rein, N. Solladié, E. Rivera, *Langmuir* **2012**, *28*, 11195–11205; c) S. Kim, S.-J. Yoon, S. Y. Park, *J. Am. Chem. Soc.* **2012**, *134*, 12091–12097.
[14] a) A. D. Guerzo, A. G. L. Olive, J. Reichwagen, H. Hopf, J.-P. Desvergne, *J. Am. Chem. Soc.* **2005**, *127*, 17984–17985; b) A. Ajayaghosh, C. Vijayakumar, V. K. Praveen, S. S. Babu, R. Varghese, *J. Am. Chem. Soc.* **2006**, *128*, 7174–7175; c) A. G. L. Olive, A. D. Guerzo, C. Schafer, C. Belin, G. Raffy, C. Giansante, *J. Phys. Chem. C.* **2010**, *114*, 10410–10416; d) K. V. Rao, K. K. R. Datta, M. Eswaramoorthy, S. J. George, *Chem. Eur. J.* **2012**, *18*, 2184–2194; e) Y. Ren, W. H. Kan, V. Thangadurai, T. Baumgartner, *Angew. Chem. Int. Ed.* **2012**, *51*, 3964–3968.
[15] L. Chen, S. Revel, K. Morrisb, D. J. Adams, *Chem. Commun.* **2010**, *46*, 4267–4269.
[16] H. Kashida, T. Takatsu, K. Sekiguchi, H. Asanuma, *Chem. Eur. J.* **2010**, *16*, 2479–2486.
[17] M. Soleimani, J. C. Haley, D. Majonis, G. Guerin, W. Lau, M. A. Winnik, *J. Am. Chem. Soc.* **2011**, *133*, 11299–11307.
[18] a) M. Durmus, J. Y. Chenc, Z. X. Zhaoa, T. Nyokong, *Spectrochim. Acta Part A.* **2008**, *70*, 42–49; b) G. Zaragoza-Galán, M. A. Fowler, J. Duhamel, R. Rein, N. Solladié, E. Rivera, *Langmuir* **2012**, *28*, 11195–11205; c) S. Kim, S.-J. Yoon, S. Y. Park, *J. Am. Chem. Soc.* **2012**, *134*, 12091–12097.
[19] a) S. Halivni, A. Sitt, I. Hadar, U. Banin, *ACS Nano* **2012**, *6*, 2758–2765; b) K.-S. Kim, J.-H. Kim, H. Kim, F. Laquai, E. Arifin, J.-K. Lee, S. I. Yoo, B.-H. Soh, *ACS Nano* **2012**, *6*, 5051–5059; c) E. I. Zenkevich, A. P. Stupak, D. Kowerko, C. Borczyskowski, *Chem. Phys.* **2012**, *406*, 21–29.
[20] Y. Okahata, H. Ihara, T. Kunitake, *Bull. Chem. Soc. Jpn.* **1981**, *54*, 2072–2078.
[21] a) T. Trupkea, A. Shalava, B. S. Richardsa, P. Wurfelb, M. A. Green, *Sol. Energy Mater. Sol. Cells* **2006**, *90*, 3327–3338; c) B. S. Richards, *Sol. Energy Mater. Sol. Cells* **2006**, *90*, 2329–2337; c) M. J. Currie, J. K. Mapel, T. D. Heidel, S. Goffri, M. A. Baldo, *Science* **2008**, *321*, 226–228.